HHS Public Access

Author manuscript

Cell Rep. Author manuscript; available in PMC 2019 August 21.

Published in final edited form as:

Cell Rep. 2019 August 06; 28(6): 1455–1470.e4. doi:10.1016/j.celrep.2019.07.004.

Select Septate Junction Proteins Direct ROS-Mediated Paracrine Regulation of *Drosophila* Cardiac Function

Hui-Ying Lim[1,3,*], **Hong Bao**[1], **Ying Liu**[1], **Weidong Wang**[2]

[1]Department of Physiology, University of Oklahoma Health Science Center, Oklahoma City, OK, USA

[2]Department of Medicine, Section of Endocrinology, University of Oklahoma Health Sciences Center, Oklahoma City, OK, USA

[3]Lead Contact

SUMMARY

Septate junction (SJ) complex proteins act in unison to provide a paracellular barrier and maintain structural integrity. Here, we identify a non-barrier role of two individual SJ proteins, Coracle (Cora) and Kune-kune (Kune). Reactive oxygen species (ROS)-p38 MAPK signaling in non-myocytic pericardial cells (PCs) is important for maintaining normal cardiac physiology in *Drosophila*. However, the underlying mechanisms remain unknown. We find that in PCs, Cora and Kune are altered in abundance in response to manipulations of ROS-p38 signaling. Genetic analyses establish Cora and Kune as key effectors of ROS-p38 signaling in PCs on proper heart function. We further determine that Cora regulates normal Kune levels in PCs, which in turn modulates normal Kune levels in the cardiomyocytes essential for proper heart function. Our results thereby reveal select SJ proteins Cora and Kune as signaling mediators of the PC-derived ROS regulation of cardiac physiology.

In Brief

Lim et al. report a non-barrier function of two select septate junction proteins, Cora and Kune, in *Drosophila* pericardial cells (PCs). Cora and Kune serve as effectors of physiological reactive oxygen species signaling in PCs to direct paracrine regulation of proper cardiac function.

Graphical Abstract

[*]Correspondence: hlim@ouhsc.edu.

AUTHOR CONTRIBUTIONS

H.-Y.L. supervised the project, designed and performed most of the experiments, analyzed data, and wrote the paper. H.B. performed experiments. Y.L. performed experiments. W.W. designed experiments, analyzed data, and wrote the paper.

SUPPLEMENTAL INFORMATION

Supplemental Information can be found online at https://doi.org/10.1016/j.celrep.2019.07.004.

DECLARATION OF INTERESTS

The authors declare no competing interests.

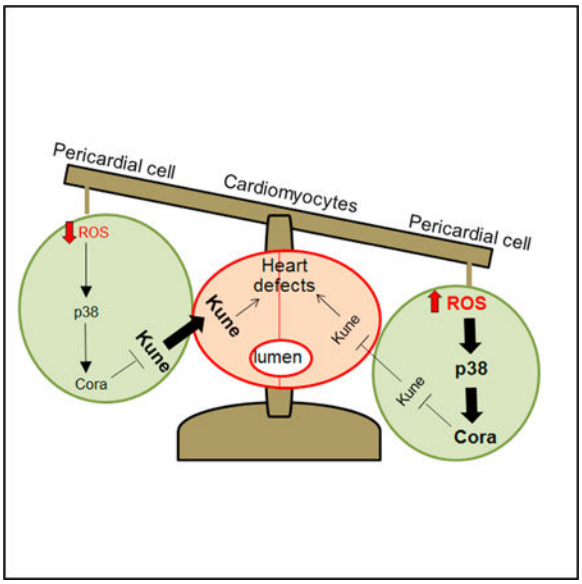

INTRODUCTION

Cell-cell interaction is typically maintained and regulated by various multi-protein complexes such as tight junctions, adherens junctions (AJs), and gap junctions. Invertebrate septate junctions (SJs), which have functional and molecular similarity to vertebrate tight junctions (TJs), are specialized, multi-protein junctional complexes that reside between the apposed plasma membranes of adjacent epithelial cells. In *Drosophila*, more than 20 molecular constituents of the SJ have been identified, and characterization of these proteins reveals their canonical role in in sealing neigh-boring cells and restricting the free diffusion of solutes between adjacent cells, thereby providing a paracellular permeability barrier (Beyenbach, 2003; Ganot et al., 2015; Izumi et al., 2016; Knust and Bossinger, 2002; Skaer and Maddrell, 1987; Tepass et al., 2001). The SJ protein complex is also involved in the coordinated changes in cell shape and rearrangement during tissue morphogenesis at a stage when the SJ structure has not yet formed or matured to become optically visible. For instance, mutations in all tested SJ genes cause defects in head involution, dorsal closure, and salivary gland elongation during early embryonic development before a clear SJ structure has been formed (Baumgartner et al., 1996; Fehon et al., 1994; Hall and Ward, 2016). Mutations in all tested SJ genes also cause cell-cell dissociation in the *Drosophila* embryonic heart, a tissue that seemingly lacks discernable SJs (Rugendorff et al., 1994; Yi et al., 2008). Although most studies on the SJ proteins are focused on their canonical barrier function, it has been known that subsets of SJ proteins may have a different, non-barrier role. For instance, the SJ proteins Neurexin-IV (Nrx-IV), the Na^+K^+ATPase β subunit Nervana 2 (Nrv2), Coracle (Cora), and Yurt form a group with a distinct role in promoting epithelial apical-basal polarity (Laprise et al., 2009). SJ components have also recently been found to play a role in regulating Hippo signaling to control intestinal stem cell activity (Xu et al., 2019) and hematopoiesis (Khadilkar and Tanentzapf, 2019). Together, these findings support the emerging notion that SJ proteins could serve important roles beyond their canonical

barrier function. However, the non-barrier functions of the SJ proteins and the individual SJ proteins that could be involved remain poorly understood.

The heart is a heterogeneous organ comprising the contractile cardiomyocytes (CMs) and non-myocytes, such as the epicardial cells and endocardial cells. The non-myocytes have important signaling roles that contribute to CM development, growth, and function (Smith and Bader, 2007). The *Drosophila* heart is a linear tube comprising two inner rows of contractile CMs closely flanked by two outer rows of non-myocytic pericardial cells (PCs; see Figure S1I). PCs have been characterized as nephrocytes that are analogous to the mammalian podocytes that function to filter toxins and proteins from the hemolymph, the equivalent of mammalian blood (Das et al., 2008; Fife et al., 1987; Helmstädter et al., 2017; Mills and King, 1965; Na et al., 2015; Tutor et al., 2014; Weavers et al., 2009; Wigglesworth, 1970; Zhuang et al., 2009). The PC nephrocytes are characterized by an intricate cell shape that includes elongated infoldings of the plasma membrane to form foot processes and labyrinthine channels. The labyrinthine channels are sealed by the slit diaphragm, which is a highly organized structure composed of similar proteins as the slit diaphragm in mammals (Ivy et al., 2015; Mallipattu et al., 2012; Weavers et al., 2009; Zhuang et al., 2009). The slit diaphragm serves as a filtration barrier to control the inflow of certain substances into the labyrinthine channels from the hemolymph. In addition, vesicular invaginations of the plasma membrane occur along the labyrinthine channels that are indicative of endocytosis of the sequestered materials from the hemolymph (Lehmacher et al., 2009). Materials endocytosed into the nephrocytes, presumably toxic molecules from the hemolymph, are targeted for either degradation in the lysosome or recycling back to the hemolymph (Helmstädter et al., 2017; Zhang et al., 2013). Moreover, the CMs and PCs are separated by a basement membrane composed of extracellular matrix (ECM), which could serve as a filtration system for hemolymph content (Psathaki et al., 2018).

On the other hand, accumulating evidence is indicating an important secretory function of PC nephrocytes. An early observation of an increased synthesis of the bactericidal enzyme lysozyme in PCs following the experimental infection of the insect *Calliphora erythrocephala* with bacteria (Crossley, 1972) provided the first indication that PCs could manufacture proteins for release into the hemolymph. More recently, *Drosophila* PCs have been reported to secrete factors, such as the ECM components and hemolymph proteins that could directly control neighboring CM function (Drechsler et al., 2013; Psathaki et al., 2018; Wilmes et al., 2018). In addition, PCs have been reported to produce reactive oxygen species (ROS) under normal, non-stressed conditions (Lim et al., 2014). ROS belong to a group of reactive chemical species produced by the incomplete reduction of molecular oxygen and are now recognized to serve an important role in the regulation of various cardiac physiological processes (Shimokawa, 2013; Taverne et al., 2013; Vara and Pula, 2014). Physiological ROS produced in the PCs of the *Drosophila* heart control the production of downstream signals such as D-p38 MAPK in PCs that then act in a paracrine manner to regulate CM function and morphology (Lim et al., 2014). The phenomenon is apparently conserved, as a study on the zebrafish heart reported that injury-induced H_2O_2 in the epicardial cells promotes the regeneration of the neighboring myocardium through the activation of ERK1/2 MAPK signaling and likely the generation of soluble factors from the epicardial cells (Han et al., 2014). Together, these findings support the notion that a

conserved ROS-MAPK signaling axis operates in the epi-or pericardium to influence myocardial function. However, the molecular mechanisms underlying ROS-MAPK-mediated paracrine interactions are currently unknown.

In this study, we found that among the SJ proteins tested in adult PCs, only Cora and Kune-kune (Kune) are altered in abundance by ROS-D-p38 signaling in PCs. Our results further showed that pericardial ROS-D-p38 signaling regulates CM function and structure through Cora and Kune. We also found that Cora controls Kune amount in PCs and that pericardial Kune in turn modulates myocardial Kune expression that is essential for normal cardiac physiology. Our study thereby unravels an unexpected function of the select SJ proteins Cora and Kune as physiological signaling mediators in PCs, a role that is distinct from their common primary barrier function.

RESULTS

Cora and Kune Abundance Is Regulated by ROS Levels in Pericardial Cells

To investigate the molecular basis of paracrine cardiac regulation by ROS-D-p38 signaling in PCs, we sought to elucidate the downstream targets of ROS-D-p38 in PCs. We reasoned that pericardial-derived ROS signaling could influence CM function by modulating the expression levels of proteins in PCs that are in contact with the CMs. We therefore used a candidate-based strategy focusing on some canonical membrane and membrane-associated junction proteins that are known to be present in the *Drosophila* heart and examined their expression in response to changing ROS levels in PCs. We first overexpressed the ROS-scavenging enzyme catalase (Nimse and Pal, 2015) using the *Gal4/UAS* system (Phelps and Brand, 1998), which reduces pericardial ROS levels by ~40% relative to control PCs (Figures S1A, S1B, and S1D). Examination of several members of the *Drosophila* protein 4.1 superfamily, which comprises membrane-associated proteins that localize to the cytoplasmic face of the plasma membrane (Fehon et al., 1994; Lamb et al., 1998), led to the observation that only Cora and not Moesin or Talin responds to decreases in ROS levels (Figures S1J, S1J′, S1K, S1K′, S1L, and S1L′). Under normal condition, Cora is localized to the periphery of PCs (Figures 1A and 1A′). A reduction in pericardial ROS level causes decreased concentrations of peripheral Cora compared with control PCs at 7 days (by ~50%; Figures S2A, S2A′, and S2B), 14 days (by ~50%; Figures 1A–1B′ and 1D), and 21 days (by ~40%; Figures S2C, S2C′, and S2D) of adulthood. In addition, use of a different PC-specific *Gal4* driver, *Sns-Gal4* (Zhuang et al., 2009), to induce catalase overexpression similarly attenuates the peripheral level of Cora compared with control PCs (by ~55%; Figures S2E, S2E′, and S2F). To ascertain that the observed effects on peripheral Cora expression was due to changing pericardial ROS levels and not to catalase-specific function, we examined Cora content in the periphery of PCs bearing alterations in the level of superoxide dismutases 1 and 2 (sod1 and sod2), another class of ROS-scavenging enzymes (Kanzaki et al., 2017). We found that over-expression of sod1 and sod2 in PCs leading to the suppression of pericardial ROS (by ~40% compared with control PCs; Figures S1E, S1F, and S1H) was associated with diminished amounts of peripheral Cora (by ~50% compared with control PCs; Figures S2G, S2G′, and S2H) in 14-day-old hearts. Therefore, ROS level

selectively regulates the abundance of Cora but no other tested protein 4.1 family members in PCs.

As Cora is a well-established component of the SJ complex (Fehon et al., 1994), we sought to investigate whether decreasing ROS levels also affects other SJ proteins, such as the four-pass transmembrane Claudin family members (Sinuous [Sinu], Kune, and Megatrachea [Mega]; Behr et al., 2003; Nelson et al., 2010; Wu et al., 2004) and the single-pass transmembrane proteins (Nrx-IV and Nrv2; Baumgartner et al., 1996; Genova and Fehon, 2003). Among the tested SJ proteins, only Kune was responsive to the dampening of ROS levels in PCs (Figures S1M, S1M′, S1N, S1N′, S1O, S1O′, S1P, S1P′, S1Q, and S1Q′). We found that whereas overall, Kune level in catalase-overexpressing PCs was moderately raised compared with that of control PCs at 7 days of adulthood (by ~20%; Figures S2I, S2I′, and S2J), it became strongly and significantly higher relative to control PCs at 14 days (by ~50%; Figures 1E–1F′ and 1H) and 21 days (by ~40%; Figures S2K, S2K′, and S2L) of adulthood. Likewise, there was a significant increase in Kune level in sod1-overexpressing PCs (by ~48%; Figures S2M, S2M′, and S2N). We conclude that manipulations of ROS to sub-physiological level only alter the levels of Cora and Kune (and not other tested SJ proteins) in PCs.

We next examined the effects of increasing ROS levels on the quantities of Cora, Kune, and other SJ proteins in PCs. When we elevated pericardial ROS levels (by ~75% compared with control PCs; Figures S1A, S1C, and S1D) by knocking down *catalase* using RNAi, we observed that pericardial Cora content was moderately but significantly enhanced compared with control PCs at 7 days (by ~25%; Figures S2A, S2A″, and S2B) but robustly increased at 14 days (by ~75%; Figures 1A, 1A′, 1C, 1C′, and 1D) and 21 days (by ~2-fold; Figures S2C, S2C″, and S2D) of adult-hood. Moreover, use of *Sns-Gal4* to induce *catalase* silencing in PCs similarly boosted peripheral Cora levels compared with control PCs in 14-day-old adult hearts (by ~3-fold; Figures S2E, S2E″, and S2F). Last, silencing of both *sod1* and *sod2* in PCs leading to heightened pericardial ROS levels (by ~3-fold; Figures S1E, S1G, and S1H) similarly caused an accumulation of pericardial Cora amounts compared with control PCs in 14-day-old hearts (by ~75%; Figures S2G, S2G″, and S2H). In contrast, Kune content was diminished in *catalase*-silenced PCs compared with control PCs at 7 days (by ~50%; Figures S2I, S2I″, S2J), 14 days (by ~70%; Figures 1E, 1E′, 1G, 1G′, and 1H), and 21 days (by ~60%;Figures S2K,S2K″, and S2L)ofadult-hood, as well as in *sod1*- and *sod2*-silenced PCs (by ~50% compared with control PCs; Figures S2M, S2M″, and S2N). On the other hand, we did not detect obvious changes in the quantities of other protein 4.1 family members and SJ proteins, including Moesin and Talin (Figures S1J″ and S1K″), Mega, Sinu, Nrx-IV, Nrv2 (Figures S1M″;, S1N″, S1O″, and S1P″), the glycosylphosphatidyl-inositol (GPI)-anchored protein Contactin (Faivre-Sarrailh et al., 2004) (Figures S1R and S1R′), and the guanylate kinase homolog Disc-large (Woods et al., 1997) (Figures S1S and S1S′), in the *catalase*-knockdown PCs compared with control PCs. Furthermore, the level of Armadillo (Arm), the *Drosophila* homolog of mammalian β-catenin and a component of the AJ, in the PC periphery also seemed unaffected by an increase in pericardial ROS level (Figures S1T and S1T′). Taken together, our findings indicated that Cora and Kune are the only SJ proteins among those tested in which their protein levels are altered upon the manipulations of ROS to sub- or supra-physiological

levels in PCs. Interestingly, our results also showed that ROS positively regulate the level of Cora but negatively regulate the level of Kune in PCs (Figure 1).

Cora Acts in Pericardial Cells to Regulate Cardiomyocyte Function

Next, we sought to determine whether Cora and Kune, whose expression levels are regulated by ROS level in PCs, also function in PCs to elicit the paracrine regulation of proper heart function and morphology, as seen for pericardial ROS (Lim et al., 2014). We first performed Cora loss-of-function manipulations in PCs, followed by adult heart function analysis (Fink et al., 2009; Ocorr et al., 2007b). We found that targeted knockdown of *cora* by RNAi in PCs using either the *Dot-Gal4* (leading to ~75% reduction in Cora level relative to control PCs; Figures 2A–2B′ and 2D) or *Sns-Gal4* driver led to a deterioration in normal heart rhythm compared with control flies, as seen by the increased incidence of irregular heartbeats (Figures 2E, 2E′, S3A, and S3A′), broader distribution of heart periods (HPs; Figures 2F, 2F′, S3B, and S3B′), and significantly increased arrhythmia index (AI) at both 1 and 4 weeks of adulthood (Figures 2G and S3C). The pericardial-specific *cora*-knockdown flies also displayed increased HP compared with control flies at 1 and/or 4 weeks of age (Figures 2F, 2F′, 2H, S3B, S3B′, and S3D) that was due primarily to a lengthening of the diastolic interval (Figure S3G). Furthermore, flies with PC-specific knockdown of *cora* exhibited significant reductions in both diastolic and systolic heart diameters compared with control flies at 1 week of age (Figures 2I, 2J, S3E, and S3F). At 4 weeks of age, no significant difference between the *Dot-Gal4 > cora*^{RNAi} or *Sns-Gal4 > cora*^{RNAi} hearts and their respective control hearts were detected (Figures 2I, 2J, S3E, and S3F), suggesting that progressive dilation of the cora-knockdown hearts has occurred resulting in a relief of the initial (1-week-old) heart tube narrowing.

We then performed Cora gain-of-function experiments by overexpressing wild-type Cora (Cora^{+}) specifically in PCs, followed by adult heart function analyses. We observed that PC-specific overexpression of Cora^{+}, leading to ~70% increase in Cora level relative to control PC (Figures 2A, 2A′, 2C, 2C′, and 2D), evoked a higher frequency of irregular heartbeats (Figures 2E and 2E″), broader distribution of HPs (Figures 2F and 2F″), and significantly increased AI (Figure 2G). The HP in flies with PC-specific overexpression of Cora^{+} was also decreased compared with control hearts at 1 and 4 weeks old (Figures 2F, 2F″, and 2H), primarily because of a shortening of the diastolic interval (Figure S3H). This is in contrast to the PC-targeted *cora*-silenced hearts at 1 and 4 weeks old, whereby their HPs were significantly greater than that of control hearts (Figure 2H). Diastolic and systolic diameters of the pericardial Cora-overexpressing hearts were also significantly lowered compared with control hearts at 1 and 4 weeks old (Figures 2I and 2J), thus indicating a chronic restriction of the heart tube, which is unlike the pericardial *cora*-silenced hearts that display a progressive expansion from 1 to 4 weeks old (Figures 2I and 2J).

To further examine whether the gain and loss of function of pericardial Cora only during the adult stage would elicit cardiac phenotypes, we used the inducible Gal80^{ts} system (Osterwalder et al., 2001) to evoke Cora overexpression or knockdown specifically in PCs only at the onset of adulthood, followed by heart functional analyses at about 1 and/or 4 weeks subsequent. We observed significant increases in AI in the adult-only pericardial Cora

$^{+}$-overexpressing or *cora*-knockdown flies, compared with control flies (Figure 2K). The adult-only pericardial *cora*-knockdown flies also exhibited significant increase in the HP relative to control flies (Figure 2L). Notably, Although the adult-only Cora^{+}-overexpressing flies displayed significant decreases in diastolic and systolic diameters compared with control flies at 1 and 4 weeks old, the adult-only pericardial *cora*-knockdown flies displayed a trend of progressive heart tube widening relative to control flies (Figures 2M and 2N) over the same period. These cardiac alterations phenocopied that seen in flies that bear similar genetic manipulations of pericardial Cora levels throughout their life cycle (Figures 2G–2J). Collectively, these data reveal an important direct role of Cora in the PCs on proper cardiac performance.

Cora Is a Functional Effector of ROS Signaling in Pericardial Cells

Our above-described cardiac defects attributed to pericardial *cora* knockdown or overexpression are reminiscent of that seen in hearts with reduced or enhanced pericardial ROS signaling, respectively (Lim et al., 2014). Together with the expression studies (Figures 1, S1, and S2), we posit that Cora serves as a functional effector of ROS signaling in PCs. To test that, we examined the epistatic relationship between ROS and Cora, first by asking whether reintroduction of Cora in PCs could rescue the cardiac dysfunction resulting from the lowering of pericardial ROS levels. Indeed, overexpression of Cora^{+} specifically in PCs that also overexpressed catalase (*Dot-Gal4 > catalase, coracle^{+}*) markedly improved the heartbeat irregularities and HP increase that were associated with the pericardial overexpression of catalase alone or with GFP, at 1 and/or 4 weeks old (Figures 3A–A″, 3B, and 3C). Co-overexpression of Cora^{+} and catalase in PCs also significantly corrected the reduced diastolic diameter (Figure 3D) and systolic diameter (Figure 3D′) that were seen in flies bearing the pericardial overexpression of catalase alone or with GFP at 1 week old.

To further determine that *cora* is epistatic to ROS in PCs, we assessed whether the cardiac abnormalities associated with supra-physiological levels of pericardial ROS can be rescued by concomitantly suppressing Cora level using two separate heterozygous *cora* mutations (*coracle^{3}* and *coracle^{5}*). We first analyzed the adult heart function of *coracle$^{3/+}$* and *coracle$^{5/+}$* flies and detected cardiac abnormalities that were reminiscent of those seen in the pericardial *cora*-knockdown flies (Figure 2), including significant increases in the AI (Figure 3F) and HP (Figure 3G) relative to control flies. Moreover, the expanded heart tube phenotype seen in the pericardial *cora*-knockdown flies during late adulthood (4 weeks; Figures 2I and 2J) was already evident in 1-week-old *coracle$^{3/+}$* and *coracle$^{5/+}$* flies and became more pronounced by 4 weeks of age (Figures 3H and 3I). Importantly, we found that the *cora* alleles were sufficient to significantly (*coracle^{3}*) or partially (*coracle^{5}*) restore the normal heart rhythm (Figures 3E–3E″ and 3F) and HP (Figure 3G) of hearts bearing the pericardial silencing of *catalase* at 1 week old. Additionally, at 1 week old, the *coracle^{3}* or *coracle^{5}* mutation significantly restored the normal morphology (diastolic and systolic diameters) of the pericardial *catalase*-knockdown hearts (Figures 3H and 3I). At 4 weeks old, the pericardial *catalase*-knockdown hearts, like the *cora*-knockdown hearts (Figures 2I and 2J), continued to be more constricted than the control heart; however, this heart tube thinning phenotype could be improved in the presence of *coracle^{3}* (significantly in the case for diastolic diameter) or *coracle^{5}* heterozygosity (Figures 3H and 3I). In sum, these data

suggested that Cora is critical for the paracrine effects of pericardial ROS on cardiac physiology.

Cora Acts Downstream of D-p38 Signaling in Pericardial Cells to Regulate Normal Cardiac Function

We have previously shown that ROS control the activity of D-p38 in PCs to elicit the paracrine modulation of CM function (Lim et al., 2014). To investigate whether Cora also acts downstream of D-p38 in the governance of CM function from the PCs, we first determined whether Cora amounts in the PCs could be regulated by D-p38 activity, by assessing whether loss of the two *Drosophila* p38 genes, *D-p38a* and *D-p38b*, could alter Cora content in PCs. Indeed, we found that the overexpression of a dominant-negative form of D-p38b (*D-p38b*^{DN}) resulted in diminished amounts of Cora in PC surfaces relative to control PCs as that seen in the catalase-overexpressing PCs (by ~40% for D-p38b^{DN} and ~50% for catalase overexpression; Figures S4A–S4C and S4E). Moreover, there was a visible reduction in peripheral Cora level in the PCs of 7-day-old *D-p38a,b* double-mutant hearts (by ~60% compared with wild-type hearts; Figures S5A and S5C). Therefore, p38 signaling, like ROS, is important in maintaining normal levels of Cora in the PCs.

To determine whether p38 signaling mediates the ROS modulation of normal Cora levels in PCs, we found that diminished levels of Cora in the periphery of the catalase-overexpressing PCs compared with control PCs (Figures S4A and S4B) could be partially yet significantly restored by the co-overexpression of a wild-type *D-p38b*$^{+}$ transgene (*Dot-Gal4 > catalase, D-p38b*$^{+}$; Figures S4B, S4D, and S4E). Conversely, in *catalase*- silenced PCs, which exhibited a robust increase in pericardial Cora content relative to control PCs (by ~1.9-fold; Figures S4F, S4G, and S4J), overexpression of *D-p38b*^{DN} significantly suppressed the accumulation of Cora (compare Figures S4G, S4I, and S4J). These results suggested that ROS act through D-p38 signaling to regulate normal levels of Cora in PCs.

We further examined the functional relationship between D-p38 signaling and Cora in regulating CM function from PCs. We have previously shown that inhibition of D-p38 signaling in PCs led to cardiac defects that mimicked those seen in hearts with diminished pericardial ROS concentrations, including deterioration of normal cardiac rhythm and heart tube remodeling (initial narrowing of heart tube followed by heart tube expansion) at 1 and 4 weeks old (Lim et al., 2014). Hence, we reasoned that if Cora functions downstream of D-p38 in PCs, the cardiac abnormalities caused by impaired or enhanced D-p38 signaling activity should be rescued by Cora upregulation or *cora* deficiency, respectively. Indeed, replenishment of Cora amount in the *D-p38b*^{DN}-overexpressing PCs, via overexpression of Cora^{+}, rescued the deterioration in heartbeat regularity caused by impaired pericardial D-p38 signaling to a level comparable with that of the control at 1 week old (Figures S4K–S4K″ and S4L). In addition, we found that overexpression of *D-p38b*$^{+}$ specifically in PCs, although not eliciting an obvious increase in Cora content compared with control PCs (Figures S4F, S4H, and S4J), caused a significant reduction in diastolic and systolic diameters compared with control flies at 1 week old, which could be corrected by a heterozygous *coracle*^{3} or *coracle*^{5} mutation (Figure S4M). Collectively, these genetic

interaction data positioned Cora functionally downstream of ROS-D-p38 signaling cascade in PCs.

The Abundance of Kune in Pericardial Cells Is Controlled by ROS-D-p38-Cora Signaling Level

Our results revealed that in addition to Cora, another SJ protein, Kune, was regulated by ROS in PCs (Figures 1, S1, and S2). We therefore determined whether Kune level in PCs could also be regulated by D-p38 and Cora. We observed that Kune abundance was significantly enhanced in the PCs of *D-p38a,b* double-mutant hearts compared with wild-type hearts (by~2.5-fold; Figures S5D–S5F) and in PCs that overexpressed $D\text{-}p38b^{DN}$ compared with control PCs at 7 days of adulthood (by ~30%; Figures 4A–4B′ and 4D). Conversely, $D\text{-}p38^{+}$-overex-pressing PCs displayed moderately reduced quantities of Kune in their peripheries compared with control PCs (by ~25%; Figures 4A, 4A′, 4C, 4C′, and 4D). We next examined whether Cora, which we established to be a downstream mediator of ROS-D-p38 signaling (Figures 3 and S4), also regulates Kune level or vice versa in PCs, given that both are known to be in close physical proximity as components of the SJ complex (Oshima and Fehon, 2011). We observed that the $coracle^{3/+}$ and $coracle^{5/+}$ heterozygous hearts exhibited gains in pericardial Kune levels relative to wild-type hearts (by ~2- to 2.5-fold; Figures S5G–S5J). Moreover, there was an increase in Kune levels in *cora*-silenced PCs compared with control PCs (by ~55%; Figures 4E–4F′ and 4H). Conversely, we detected a decrease in Kune content in the $Cora^{+}$-overexpressing PCs relative to control PCs (by ~35%; Figures 4E, 4E′, 4G, 4G′, and 4H). Therefore, Cora, like ROS and D-p38, is crucial in maintaining normal Kune quantities in PCs. In contrast, loss-or gain-of-function manipulation of Kune in PCs did not appear to affect normal Cora level (Figures 4I–4L), suggesting that Kune does not reciprocally affect Cora amount in PCs.

We further investigated whether the ROS control of Kune abundance is mediated through Cora. For that, we determined whether the reduced quantity of Kune seen in PCs with elevated ROS levels (and consequently heightened Cora levels) could be rescued by the concomitant blunting of Cora levels in those PCs. Indeed, we found that whereas PC-specific silencing of *catalase* significantly diminished pericardial Kune levels compared with control PCs (by ~70%; Figures S6A, S6B, and S6E), Kune levels were restored to 65%–80% of the normal levels in the presence of heterozygous *cora* mutation (PC-specific $catalase^{RNAi}$ in $coracle^{3}$ or $coracle^{5}$ background) (Figures S6C–S6E), suggesting that ROS act through Cora to maintain normal levels of Kune in the PC surfaces.

Kune Acts Downstream of ROS-D-p38-Cora in Pericardial Cells to Regulate Cardiac Function

Cora is a SJ protein that localizes to the cytosolic face of the plasma membrane (Fehon et al., 1994; Ward et al., 1998). Therefore, for Cora in the PC to modulate CM function in a paracrine manner, it is likely to act indirectly through another factor, for instance a transmembrane protein residing in the surface membrane of PCs that can directly engage the CMs. As Kune is a trans-membrane protein (Nelson et al., 2010), and its content in the surfaces of PCs was found to be regulated by ROS-D-p38-Cora level, it is conceivable that Kune serves as a functional effector of ROS-D-p38-Cora signaling axis in PCs. To test this

possibility, we first examined whether CM function was affected by decreasing Kune level specifically in PCs (by ~30% compared with control PCs; Figures 5A–5B′ and 5D). We found that relative to control flies, the *kune*-knockdown flies exhibited increased heart arrhythmicity (Figures 5E, 5E′, 5F, and 5F′) that reached significance at 3 weeks old (Figure 5G), as well as significant reductions in the heart tube dimensions at 1 and 3 weeks old (Figures 5H and 5I). These cardiac defects are reminiscent of those deficits displayed by hearts with increased Cora levels (Figure 2), elevated ROS concentrations (Figure 3; Lim et al., 2014), and heightened D-p38 activity (Figure S4; Lim et al., 2014) in PCs. On the other hand, hearts with PC-specific overexpression of $kune^{+}$, which increased Kune abundance by ~55% compared with control PCs (Figures 5A, 5A′, 5C, 5C′, and 5D), displayed an increased frequency of irregular heartbeats (Figures 5E″, 5F″, and 5G) and significant increases in HP (Figure 5F″) compared with control hearts (Figures 5E–5G) at 1 and 3 weeks old. The diastolic and systolic diameters of the $kune^{+}$-overexpressing hearts were comparable with those of control hearts at 1 week old but became significantly greater than control hearts at 3 weeks old (Figures 5H and 5I), thus exhibiting a trend of progressive heart tube widening over time. In all, these cardiac deficits mimic those seen in hearts with reduced Cora content (Figure 2), decreased ROS concentrations (Figure 3; Lim et al., 2014), and blunted D-p38 activity (Figure S4; Lim et al., 2014) in PCs. Therefore, there is a close correlation between pericardial Kune abundance changes and heart function alterations in both young (1 week old) and old (3–4 weeks old) flies. Collectively, our findings are consistent with the notion that Kune serves as a functional effector of ROS-D-p38-Cora signaling in PCs.

To further investigate whether adult-only alterations in pericardial Kune level also elicit CM functional changes, like that seen for adult-only pericardial Cora changes (Figures 2K–2N), we inhibited or overexpressed Kune in PCs only at the onset of adulthood, followed by heart functional analyses at about 1 and/or 4 weeks subsequent. We detected significant deterioration of heartbeat regularity in these flies compared with control flies at 4 weeks old (Figure 5J). In addition, adult-only pericardial *kune*-silenced flies exhibited chronic narrowing of the heart tube, with significant reduction in both diastolic and systolic diameters compared with control flies at 1 and 4 weeks old (Figures 5K and 5L). On the other hand, whereas adult-only Kune-overexpressing flies exhibited diastolic and systolic diameters that were significantly lower than those of control flies at 1 week of age, both the diastolic and systolic dimensions were comparable with those of control flies at 4 weeks old (Figures 5K and 5L), thus indicative of a progressive heart tube expansion phenotype. Together, these results mimic those observed in flies bearing similar genetic manipulations of pericardial Kune levels throughout their life cycle (Figures 5G–5I), thereby identifying an important direct role of Kune in PCs on heart function regulation.

To establish that Kune elicits the ROS-D-p38-Cora signaling in PCs on CM regulation, we investigated whether the cardiac deficits associated with the gain of Cora in PCs, which caused a decrease in pericardial Kune levels compared with control PCs (by ~50%; Figures S6F, S6F′, and S6G), could be rescued by co-overexpressing Kune (Figures S6F, S6F″, and S6G). Indeed, the *Dot-Gal4 > coracle*$^{+}$*, kune*$^{+}$ flies restored the increased heart arrhythmia (Figures S6H–S6H″, S6I–S6I″, and S6J), lowered HP (Figures S6I–S6I″ and S6K), and reduced diastolic and systolic diameters (Figure S6L) that were associated with the *Dot-*

Gal4 > coracle^{+} flies to normality. In sum, these results strongly support Kune as a functional effector of ROS-D-p38-Cora signaling control of normal cardiac function from the PCs.

Next, we asked whether other SJ proteins, even though their protein abundances were not under the control of ROS level in PCs (Figure S1), could also confer the ROS regulatory effects on cardiac function. If that is the case, concomitant silencing of these genes and *catalase* in the PCs would alter the cardiac phenotypes exhibited by the pericardial *catalase*-silenced hearts. The RNAi-mediated knockdown of *nrv2* and *nrx-IV* specifically in PCs yielded approximately 90% and 40% reduction in transcript levels, respectively (Figures S7A and S7B). When we silenced *nrv2* or *nrx-IV* with *catalase* in the PCs, we detected no significant difference in the cardiac arrhythmicity in the double-knockdown hearts compared with the pericardial *catalase*-silenced hearts (Figure S7C). Moreover, the diastolic and systolic dimensions exhibited by the double-knockdown hearts were comparable with the pericardial *catalase*-silenced hearts (Figures S7D and S7E). These results suggest that although alterations of other SJ proteins such as Nrv2 or Nrx-IV could affect proper heart function (Yi et al., 2008), their effects are independent of pericardial ROS signaling function. These data further corroborate the notion that ROS-based paracrine regulation of CM function is selectively driven by Cora and Kune.

Kune Regulates Its Own Level between Neighboring Cells in the Heart but Not in the Epithelia

We further wonder how Kune in the surfaces of PCs could influence CM performance. One possibility is by modulating Kune abundance in CMs. To address that, we targeted Kune overexpression in the PCs with either *Dot-Gal4* (Figures S8A and S8B, arrows) or *Sns-Gal4* (Figures S8C and S8D) and observed moderate but detectable increases in Kune abundance in CMs (outlined by dotted lines in Figures S8A–S8D). Likewise, using *Hand-Gal4*, a driver that directs gene expression specifically in the CMs during both larval (data not shown) and adult stages (Figures S8E and S8E′), and another heart-specific driver, *TinC-*D*4-Gal4* (hereinafter termed *TinC-Gal4*) (Lo and Frasch, 2001), to overexpress Kune, we detected higher levels of Kune in PCs compared with control PCs (Figures S8F, S8G, S8I, and S8J, arrows), up to 25% and 28% elevation, respectively (Figures S8L and S8M). Conversely, *Hand-Gal4*- or *TinC-Gal4*-mediated knockdown of *Kune* was accompanied by a reduction in pericardial Kune level relative to control PCs (Figures S8F, S8H, S8I, and S8K, arrows), up to 45% and 32% reduction, respectively (Figures S8L and S8M). These results suggested that pericardial Kune and myocardial Kune positively regulate each other's level between the PCs and CMs. To further examine whether the observed phenomenon of Kune in one cell type affecting Kune level in another cell also occurs in tissues other than the heart, we generated Kune-overexpressing clones in the larval imaginal discs randomly using the heat shock Flip-out system (Struhl and Basler, 1993) (Figures S8N and S8M). The Kune-overexpressing clones, marked by eGFP expression, displayed an upregulation in Kune level as expected in both the eye and wing discs, but wild-type cells bordering the clones showed no detectable changes in Kune level (Figures S8N′, S8N″, S8M′, and S8M″). Therefore, Kune does not appear to elicit non-autonomy in the epithelia.

Normal Level of Kune in Pericardial Cell or Cardiomyocyte Is Essential for Normal Cardiac Function

Our results so far indicate that Kune residing in the PC surface modulates Kune abundance in the CMs, and we further asked whether that could be important in the maintenance of proper cardiac performance. If so, we reasoned that the manipulations of Kune directly in the CMs would generate cardiac phenotypes recapitulating those seen with the manipulations of Kune in PCs. To test that, we first overexpressed *kune*$^{+}$ directly in the CMs using *Hand-Gal4* and *TinC-Gal4*, followed by analysis of adult cardiac contractility. Our results showed that hearts bearing the CM-specific overexpression of Kune phenocopied the PC-specific Kune-overexpressing hearts by eliciting significant increases in AI and progressive heart tube widening from young to old age (Figures 6A–6A″). For instance, both the diastolic and systolic diameters of the PC-specific Kune-overexpressing hearts were comparable with those of control hearts at 1 week old, but became significantly greater than control hearts at 3 weeks old (Figures 6A′ and 6A″). Following a similar trend, both the diastolic and systolic dimensions of the CM-specific Kune-overexpressing hearts were lower than that of control hearts at 1 week old but became comparable with that of control hearts at 3 weeks old (Figures 6A′ and 6A″). On the other hand, the *Hand-Gal4*- or *TinC-Gal4*-specific *kune*-knockdown (*Hand-Gal4 > kune*^{RNAi} and *TinC-Gal4 > kune*^{RNAi}) hearts phenocopied hearts with the PC-targeted silencing of *kune*, as both caused significant elevations in AI and reductions in diastolic and systolic diameters at 1 and/or 3 weeks old (Figures 6B–6B″). Taken together, these results showed that PC Kune and CM Kune act in a similar manner to regulate CM function.

Perturbation of ROS, Cora, or Kune Level Disrupts Pericardial Surface Morphology

PCs have been characterized as the insect nephrocytes on the basis of their analogous features with vertebrate podocytes. We are curious about whether these features, which include the labyrinthine channels and slit diaphragm, could be affected by physiological ROS signaling pathway in PCs. We therefore inhibited pericardial ROS signaling by overexpressing catalase or knocking down *cora*, as well as knocking down *kune* specifically in PCs followed by ultrastructural analysis of PCs. As shown by our transmission electron micrographs, all the control PCs examined exhibited labyrinthine channels across nearly the entire surface and with the slit diaphragms flanking the mouth of each channel (Figures 7A, 7A′, and 7G, arrows). On the other hand, about half of the catalase-overexpressing PCs examined displayed normal surface morphology (Figures 7B, 7B′, and 7G), while the other half showed abnormal surface features, which include labyrinthine channel breakdown, loss of slit diaphragms, and a smoothing of the cell surface (Figures 7C, 7C′, and 7G). Among the *cora*-knock-down PCs examined, about 67% of the cells displayed normal surface morphology (Figures 7D, 7D′, and 7G), while 33% exhibited abnormal surface morphology (Figures 7E, 7E′, and 7G). Last, all *kune*-knockdown PCs examined showed a loss of peripheral labyrinthine channels and slit diaphragm as well as cellular surface smoothing (Figures 7F, 7F′, and 7G). Collectively, our results indicate that alteration of physiological ROS, Cora, or Kune concentration in PCs aberrantly affects PC nephrocyte surface histology. Of note, the basement membrane surrounding catalase-overexpressing, *cora*-knockdown, and *kune*-knockdown PCs appeared unaffected compared with control PCs, in terms of the thickness and uniformity along the entire PC (Figures 7A–7F′).

DISCUSSION

On the basis of the results of our study, we propose a model for the ROS-mediated paracrine regulation of cardiac physiology (Figure 6C). In PCs, physiological ROS-p38 level (Lim et al., 2014) governs Cora amount, which in turn regulates the level of Kune in the cellular surface. Peripheral Kune then directs the abundance of Kune in the CMs, which is essential for proper myocardial function and morphology. As a result, lowering of ROS-p38 signaling to sub-physiological level in PCs reduces pericardial Cora level and heightens pericardial Kune level, thereby raising Kune in CMs to a level that is detrimental to normal cardiac function. Conversely, elevating ROS-p38 signaling to supra-physiological level in PCs increases pericardial Cora quantity and diminishes pericardial Kune content, thereby suppressing Kune in the CMs to a level that perturbs normal heart function.

Our findings suggest that Cora and/or Kune serve dual roles as structural elements of the SJ complex and as downstream effectors of ROS signaling. Such a dual function of Cora or Kune is unexpected but perhaps not unprecedented. The signaling role of Cora and Kune as core SJ components appears analogous to that of Arm as a core AJ component. Within the AJ, Arm mediates cell-cell adhesion and anchoring of the actin cytoskeleton. However, upon activation by Wingless, the *Drosophila* homolog of Wnts, Arm accumulates in the cell and serves as a key effector of Wingless signal transduction (Peifer, 1995). In the case of Cora and Kune in the PCs, in response to the ROS signal, p38 is activated which then regulates the abundance and/or activity of these two individual SJ proteins. We therefore propose that Cora and/or Kune in the SJ have parallel functions as Arm in the AJ in that they serve as a structural component of the junctional complex and as downstream effector of signaling pathways.

Our results indicate that Kune level in the PC affects Kune level in the CM (Figure 6C); however, the underlying mechanism is unclear. One possibility is that pericardial Kune and cardiomyocyte Kune homotypically interact. In this scenario, one would predict that Kune is likely localized at the cell-cell interface. We did not observe this; however, it does not necessarily rule out the homotypic interaction hypothesis. It is possible that in addition to engaging in homotypic interaction to mediate ROS signaling, other obligations of Kune may cause Kune to become more evenly distributed across the cells. For instance, Kune might be involved in the nephrocytic activity of PCs, and hence localization of Kune all over the cell surface is essential to promote the uptake of materials from the hemolymph into PCs. In the myocardium, Kune might be involved in the synchronous contraction of the CMs, a process that could be facilitated by the uniform localization of Kune across the entire CM surface. Alternatively, Kune interaction between the pericardial and cardiac cells might not involve their direct homotypic interaction but rather be mediated by the basement membrane that resides between PCs and CMs, at least in certain regions of the fly heart (Hughes and Jacobs, 2017; Rotstein and Paululat, 2016). In addition, an aberrant change in the pericardial nephrocyte morphology caused by loss of pericardial Kune (Figure 7) might also alter Kune level in the CM. Last but not least, paracrine factors could be released from the PC in a Kune-controlled manner, which then influence Kune level in the CM. Regardless of whether intercellular Kune interaction occurs via direct cell-cell contact or indirect mechanisms, our results have demonstrated an interesting phenomenon by which the maintenance of normal

Kune abundance in CMs by its pericardial counterpart is essential for proper adult cardiac morphology and physiology. This further raises the question as to how Kune acts in CMs to control proper cardiac performance and morphology. One possibility is that Kune regulates ion channel level and/or activity in the CM plasma membrane, such as the transient receptor potential (TRP) family of Ca^{2+} channels. As such, alterations in the CM Kune level could perturb intracellular Ca^{2+} homeostasis, thereby disrupting proper cardiac contractility and structure. These possibilities remain to be investigated in future studies.

In summary, our findings reveal that select SJ proteins can act as signaling effectors and suggest that the SJ, like the AJ, could serve to organize signaling centers. Our work also provides important insights into the essential mechanisms of ROS-mediated non-myocyte-myocyte signaling interactions, a process that appears to be conserved between invertebrates and vertebrates.

STAR★METHODS

LEAD CONTACT AND MATERIALS AVAILABILITY

Further information and requests for resources and reagents should be directed to and will be fulfilled by the Lead Contact, Hui-Ying Lim (hlim@ouhsc.edu). This study did not generate new unique reagents.

EXPERIMENTAL MODEL AND SUBJECT DETAILS

Drosophila stocks were maintained at 25°C on a standard food recipe based on the Bloomington *Drosophila* stock center (Cornmeal, Soy Flour, Inactivated yeast, and agar). Flies were maintained on a 12 h light/dark cycle. All fly stocks used in this study are outlined in the Key Resources Table. For all heart immunostaining analyses, equal numbers of female and male hearts were dissected and examined. For optical imaging of adult hearts, ~30 female flies per genotype were analyzed. The age of flies for a given experiment is shown either in the corresponding figure, figure legend or text. For the temperature shift treatments of flies to induce transgene expression only during the adult phase (from newly-eclosed adults to 1- or 4-week-old adults), parental crosses were set up at 17°C. All subsequent processes (egg-laying, egg-hatching, larvae rearing, pupation) were maintained at 17°C until the eclosion of adult flies. The newly-eclosed adults were then collected on standard food vials, after which vials were transferred to 29°C. Adult flies were reared at 29°C for 1 week or 4 weeks before being analyzed for their cardiac function. All the overexpression and RNAi knockdown genotypes in this study are of the combination *Gal4/+;UAS/+* except for the *kune* knockdown flies, which is of the combination *Gal4/UAS;UAS/+* for v108440 and v3961.

METHOD DETAILS

Immunostaining—Third instar wandering-stage larvae and adult female flies (7–21 days old) were collected and dissected in PBS. Hearts were fixed in two different ways for different purposes – for sharper immunosignals in the PCs, hearts were fixed with a solution comprising picric acid/glacial acetic acid/formaldehyde in a ratio of 15:1:5 for 15 min at room temperature. For stronger immunosignals in the myocardium, hearts were fixed with

3.7% paraformaldehyde solution (freshly prepared) for 15 min at room temperature. After washing in PBS plus 0.1% Triton X-100 (PBT), the fixed hearts were incubated overnight at 4°C with primary antibodies diluted in PBT. Hearts were then washed with PBT and incubated for 2 hours at room temperature with the appropriate fluorescence-conjugated secondary antibodies (Jackson ImmunoResearch) diluted in PBT. Hearts were then washed again with PBT and mounted in ProLong Gold anti-fade reagent. Samples were examined under a laser confocal microscope (Olympus FV1000). The following reagents were used for immunostaining: from the Developmental Studies Hybridoma Bank - mouse anti-Cor C566.9c and c615 at 1:500, mouse anti-Nervana Nrv5F7 at 1:50, mouse anti-Disc large at 1:50, mouse anti-Armadillo at 1:50, mouse anti-ERM-1 at 1:100, and mouse anti-Talin E16B at 1:100. Other antibodies include rabbit anti-Kune at 1:500 (gift from Greg Beitel, Northwestern University, Evanston and Mikio Furuse, NIPS, Japan), rabbit anti-Sinu at 1:100 (gifts from Greg Beitel, Northwestern University, Evanston), rabbit anti-megatrachea at 1:100 (gift from Reinhard Schuh, Research Group Molecular Organogenesis, Germany), and rabbit anti-Neurexin-IV at 1:100 (gift of Manzoor Bhat, UT San Antonio, Texas). Secondary antibodies labeled with Cy3 or FITC (Jackson Immunoresearch Laboratories).

Fly heartbeat analysis—Cardiac contractility measurements on semi-intact preparations of fly hearts were performed as described previously (Fink et al., 2009). High-speed 30 s movies were recorded at a rate of > 150 frames per second using a Hamamatsu CCD camera on a Nikon 80i upright microscope with a 10x dipping immersion lens. The images were processed using Simple PCI imaging software (Compix Inc.). M-modes and quantitative data were generated using a MATLAB-based image analysis program (Fink et al., 2009). To generate the M-mode figures, a single pixel-wide column was selected from the most posterior portion of the adult heart at the abdominal A3 segment that encompassed both edges of the heart tube. The corresponding columns were cut from all movie frames and aligned horizontally according to time. Heart periods (HP) or heartbeat lengths were defined as the time between the ends of two consecutive diastolic intervals. The arrhythmia index (AI) was defined as the standard deviation of all recorded HPs for an individual fly, normalized to the median HP to compensate for variability between flies (Ocorr et al., 2007a). Diastolic and systolic diameters represent the relaxed and contracted state of the heart tube, respectively. Measurements were made in the exact same location in abdominal segment A3. High-speed 30 s movies were recorded at a rate of > 150 frames per second using a Hamamatsu CCD camera on a Nikon 80i upright microscope with a 10x dipping immersion lens. The images were processed using Simple PCI imaging software (Compix Inc.). M-modes and quantitative data were generated using a MATLAB-based image analysis program (Fink et al., 2009).

ROS detection—ROS detection with dihydroethidium (DHE) dye (Molecular Probes, Invitrogen) was performed using a published method (Owusu-Ansah and Banerjee, 2009), with minor modifications. In brief, adult fly hearts were dissected and cleaned in freshly prepared PBS and removed from the cuticle. Hearts were incubated with 30 μM DHE (freshly reconstituted in anhydrous DMSO and diluted in PBS) for 7–10 min at room temperature (RT) in the dark, washed three times with PBS for 5 min each in the dark, and

then fixed for 5 min with 7% paraformaldehyde (PFA). Hearts were mounted in ProLong Gold anti-fade reagent (Invitrogen) and examined under a laser confocal microscope (Zeiss).

Confocal Imaging and Image Analysis—Confocal imaging was performed with an Olympus FV1000 confocal microscope using a x20 air objective or x40 oil objective. The x20 objective was used to obtain primary images by taking z sections (each section 1–2 μm) from top to bottom of the hearts followed by projection of all z sections. The x40 objective was used to obtain images by taking z sections (each section 1–2 μm) from top to bottom of the hearts. The middle section from among the z stacks was selected and presented as a single optical section as the inset. For quantification of the pericardial SJ protein fluorescence and the pericardial ROS fluorescence, approximately 10 pericardial cells were analyzed from each of three adult flies per genotype. Mean intensity for each genotype is normalized to that of the control (set at 1.0). ImageJ Software Version 7.0 was used for image processing and quantification.

Transmission electron microscopy—1-week old adult *Drosophila* hearts of the respective genotypes were dissected and fixed with 4% Paraformaldehyde (EM grade), 2% Glutaraldehyde (EM grade), in 0.1M Sodium Cacodylate buffer pH 7.3 for 24 hours at room temperature on a rocker. Samples were then post fixed for 90 minutes in 1% Osmium tetroxide (OsO_4) in 0.1M Sodium Cacodylate buffer pH 7.3, and rinsed three times for five minutes each in 0.1M Sodium Cacodylate buffer pH7.3. Samples were stored in 0.1M Sodium Cacodylate buffer pH7.3 overnight on a rocker. The samples were then dehydrated in a graded acetone series. The acetone gradient was as follows; 50%, 60%, 75%, 85%, 95%, 100%. The hearts were in each concentration for 15 minutes on a rocker. Then the samples had two 15 minute treatments in 100% Propylene Oxide. Following dehydration, the samples were infiltrated in a graded Epon/Araldite (EMS) resin/Propylene Oxide series (1:3, 1:1, 3:1) for 60 minutes, overnight, and 120 minutes the following day respectfully. The samples were further infiltrated with pure resin for 45 minutes, 90 minutes, and then overnight. The hearts were then embedded in resin plus BDMA (accelerator) and polymerized at 60° C for 48 hours. Ultrathin sections were stained with Sato's Lead and Saturated Uranyl Acetate in 50% methanol before viewing on a Hitachi H7600 Transmission Electron Microscope.

Generation of clones and imaginal disc staining—To generate *kune*$^{+}$ clones that co-overexpress the GFP marker, flies of the genotype y hsp70-flp; Tub > GFP, y+ > Gal4, 20XUAS.6XGFP were crossed to flies of the genotype y; UAS-kune+ (UAS-transgene on II) balanced over the linked 2;3 chromosome balancer (CyO-TM6B). Clones were generated by heat shocking first or second instar larvae at 37°C for 15 minutes. Third instar larvae were subsequently dissected and their wing and eye imaginal discs fixed and stained by standard procedures (Zecca and Struhl, 2007a, 2007b), using rabbit anti-Kune at 1:500.

QUANTIFICATION AND STATISTICAL ANALYSIS

All data are presented as the mean ± SEM of the indicated number of replicates. Data were analyzed using the two-tailed Student's t test and $p < 0.05$ was considered statistically significant. Student's two-tailed unpaired t test assuming equal variance.

DATA AND CODE AVAILABILITY

This study did not generate/analyze dataset/code.

Supplementary Material

Refer to Web version on PubMed Central for supplementary material.

ACKNOWLEDGMENTS

We thank our colleagues Rolf Bodmer and Gary Struhl for thoughtful comments on some of the data in our paper. We are grateful to Greg Beitel (Northwestern University, Evanston, Illinois), Richard Fehon (University of Chicago), Mikio Furuse (National Institute for Physiological Sciences [NIPS], Japan), Manzoor Bhat (University of Texas [UT] San Antonio), Reinhard Schuh (Research Group Molecular Organogenesis, Germany), Rolf Bodmer (Sanford Burnham Prebys Medical Discovery Institute, San Diego, California), and Gary Struhl (Columbia University, New York) for critical stocks and antibodies. We also thank the Bloomington *Drosophila* Stock Center, the Vienna *Drosophila* RNAi Center, and the TRiP at Harvard Medical School for fly stocks. We acknowledge the Imaging Core Facility at the Oklahoma Medical Research Foundation (OMRF) for excellent technical assistance on electron microscopy and the NIH P20 grant (GM103636) supporting the Imaging Core. This work was supported by fellowships from the American Heart Association (13SDG14680005 to H.-Y.L.) and grants from the NIH (5R01HL128455 to H.-Y.L., 1P20GM103636 to H.-Y.L. and W.W., and 1R01DK116017–01A1 to W.W.).

REFERENCES

Baumgartner S, Littleton JT, Broadie K, Bhat MA, Harbecke R, Lengyel JA, Chiquet-Ehrismann R, Prokop A, and Bellen HJ (1996). A *Drosophila* neurexin is required for septate junction and blood-nerve barrier formation and function. Cell 87, 1059–1068. [PubMed: 8978610]

Behr M, Riedel D, and Schuh R (2003). The claudin-like megatrachea is essential in septate junctions for the epithelial barrier function in *Drosophila*. Dev. Cell 5, 611–620. [PubMed: 14536062]

Beyenbach KW (2003). Regulation of tight junction permeability with switch-like speed. Curr. Opin. Nephrol. Hypertens 12, 543–550. [PubMed: 12920403]

Chen JM, Xie CC, Tian LL, Hong LX, Wu XR, and Han JH (2010). Participation of the p38 pathway in *Drosophila* host defense against pathogenic bacteria and fungi. Proc. Natl. Acad. Sci. USA 107, 20774–20779. [PubMed: 21076039]

Crossley AC (1972). The ultrastructure and function of pericardial cells and other nephrocytes in an insect: Calliphora erythrocephala. Tissue Cell 4, 529–560. [PubMed: 4348054]

Das D, Aradhya R, Ashoka D, and Inamdar M (2008). Macromolecular uptake in *Drosophila* pericardial cells requires rudhira function. Exp. Cell Res. 314, 1804–1810. [PubMed: 18355807]

Drechsler M, Schmidt AC, Meyer H, and Paululat A (2013). The conserved ADAMTS-like protein lonely heart mediates matrix formation and cardiac tissue integrity. PLoS Genet. 9, e1003616. [PubMed: 23874219]

Faivre-Sarrailh C, Banerjee S, Li J, Hortsch M, Laval M, and Bhat MA (2004). *Drosophila* contactin, a homolog of vertebrate contactin, is required for septate junction organization and paracellular barrier function. Development 131, 4931–4942. [PubMed: 15459097]

Fehon RG, Dawson IA, and Artavanis-Tsakonas S (1994). A *Drosophila* homologue of membrane-skeleton protein 4.1 is associated with septate junctions and is encoded by the coracle gene. Development 120, 545–557. [PubMed: 8162854]

Fife HG, Palli SR, and Locke M (1987). A function for pericardial cells in an insect. Insect Biochem. 17, 829–840.

Fink M, Callol-Massot C, Chu A, Ruiz-Lozano P, Izpisua Belmonte JC, Giles W, Bodmer R, and Ocorr K (2009). A new method for detection and quantification of heartbeat parameters in *Drosophila*, zebrafish, and embryonic mouse hearts. Biotechniques 46, 101–113. [PubMed: 19317655]

Ganot P, Zoccola D, Tambutté E, Voolstra CR, Aranda M, Allemand D, and Tambutté S (2015). Structural molecular components of septate junctions in cnidarians point to the origin of epithelial junctions in eukaryotes. Mol. Biol. Evol 32, 44–62. [PubMed: 25246700]

Genova JL, and Fehon RG (2003). Neuroglian, Gliotactin, and the Na+/K+ ATPase are essential for septate junction function in *Drosophila*. J. Cell Biol. 161, 979–989. [PubMed: 12782686]

Hall S, and Ward RE (2016). Septate junction proteins play essential roles in morphogenesis throughout embryonic development in Drosophila. G3 (Bethesda) 6, 2375–2384. [PubMed: 27261004]

Han P, Zhou XH, Chang N, Xiao CL, Yan S, Ren H, Yang XZ, Zhang ML, Wu Q, Tang B, et al. (2014). Hydrogen peroxide primes heart regeneration with a derepression mechanism. Cell Res. 24, 1091–1107. [PubMed: 25124925]

Helmstädter M, Huber TB, and Hermle T (2017). Using the *Drosophila* nephrocyte to model podocyte function and disease. Front Pediatr. 5, 262. [PubMed: 29270398]

Hughes CJR, and Jacobs JR (2017). Dissecting the role of the extracellular matrix in heart disease: lessons from the *Drosophila* genetic model. Vet. Sci 4, E24. [PubMed: 29056683]

Ivy JR, Drechsler M, Catterson JH, Bodmer R, Ocorr K, Paululat A, and Hartley PS (2015). Klf15 is critical for the development and differentiation of *Drosophila* nephrocytes. PLoS ONE 10, e0134620. [PubMed: 26301956]

Izumi Y, Motoishi M, Furuse K, and Furuse M (2016). A tetraspanin regulates septate junction formation in *Drosophila* midgut. J. Cell Sci. 129, 1155–1164. [PubMed: 26848177]

Kanzaki H, Wada S, Narimiya T, Yamaguchi Y, Katsumata Y, Itohiya K, Fukaya S, Miyamoto Y, and Nakamura Y (2017). Pathways that regulate ROS scavenging enzymes, and their role in defense against tissue destruction in periodontitis. Front. Physiol 8, 351. [PubMed: 28611683]

Khadilkar RJ, and Tanentzapf G (2019). Septate junction components control *Drosophila* hematopoiesis through the Hippo pathway. Development 146, 146.

Kimbrell DA, Hice C, Bolduc C, Kleinhesselink K, and Beckingham K (2002). The Dorothy enhancer has tinman binding sites and drives hop-scotch-induced tumor formation. Genesis 34, 23–28. [PubMed: 12324942]

Knust E, and Bossinger O (2002). Composition and formation of intercellular junctions in epithelial cells. Science 298, 1955–1959. [PubMed: 12471248]

Lamb RS, Ward RE, Schweizer L, and Fehon RG (1998). *Drosophila* coracle, a member of the protein 4.1 superfamily, has essential structural functions in the septate junctions and developmental functions in embryonic and adult epithelial cells. Mol. Biol. Cell 9, 3505–3519. [PubMed: 9843584]

Laprise P, Lau KM, Harris KP, Silva-Gagliardi NF, Paul SM, Beronja S, Beitel GJ, McGlade CJ, and Tepass U (2009). Yurt, Coracle, Neurexin IV and the Na(+),K(+)-ATPase form a novel group of epithelial polarity proteins. Nature 459, 1141–1145. [PubMed: 19553998]

Lee S, Bao H, Ishikawa Z, Wang WD, and Lim HY (2017). Cardiomyocyte Regulation of Systemic Lipid Metabolism by the Apolipoprotein B-Containing Lipoproteins in *Drosophila*. PloS. Genet 13, e1006555. [PubMed: 28095410]

Lehmacher C, Tögel M, Pass G, and Paululat A (2009). The *Drosophila* wing hearts consist of syncytial muscle cells that resemble adult somatic muscles. Arthropod Struct. Dev 38, 111–123. [PubMed: 18983940]

Li J, Ashley J, Budnik V, and Bhat MA (2007). Crucial role of *Drosophila* neurexin in proper active zone apposition to postsynaptic densities, synaptic growth, and synaptic transmission. Neuron 55, 741–755. [PubMed: 17785181]

Lim HY, Wang W, Chen J, Ocorr K, and Bodmer R (2014). ROS regulate cardiac function via a distinct paracrine mechanism. Cell Rep. 7, 35–44. [PubMed: 24656823]

Lo PCH, and Frasch M (2001). A role for the COUP-TF-related gene seven-up in the diversification of cardioblast identities in the dorsal vessel of *Drosophila*. Mech. Dev 104, 49–60. [PubMed: 11404079]

Mallipattu SK, Liu R, Zheng F, Narla G, Ma'ayan A, Dikman S, Jain MK, Saleem M, D'Agati V, Klotman P, et al. (2012). Kruppel-like factor 15 (KLF15) is a key regulator of podocyte differentiation. J. Biol. Chem 287, 19122–19135. [PubMed: 22493483]

Mills RP, and King RC (1965). The pericardial cells of *Drosophila* melanogaster. Q. J. Microsc. Sci 106, 261–268. [PubMed: 5865262]

Na J, Sweetwyne MT, Park ASD, Susztak K, and Cagan RL (2015). Diet-induced podocyte dysfunction in *Drosophila* and mammals. Cell Rep. 12, 636–647. [PubMed: 26190114]

Nelson KS, Furuse M, and Beitel GJ (2010). The *Drosophila* Claudin Kune-kune is required for septate junction organization and tracheal tube size control. Genetics 185, 831–839. [PubMed: 20407131]

Nimse SB, and Pal D (2015). Free radicals, natural antioxidants, and their reaction mechanisms. RSC Advances 5, 27986–28006.

Ocorr K, Perrin L, Lim HY, Qian L, Wu X, and Bodmer R (2007a). Genetic control of heart function and aging in *Drosophila*. Trends Cardiovasc. Med 17, 177–182. [PubMed: 17574126]

Ocorr K, Reeves NL, Wessells RJ, Fink M, Chen HSV, Akasaka T, Yasuda S, Metzger JM, Giles W, Posakony JW, and Bodmer R (2007b). KCNQ potassium channel mutations cause cardiac arrhythmias in *Drosophila* that mimic the effects of aging. Proc. Natl. Acad. Sci. U S A 104, 3943–3948. [PubMed: 17360457]

Oshima K, and Fehon RG (2011). Analysis of protein dynamics within the septate junction reveals a highly stable core protein complex that does not include the basolateral polarity protein Discs large. J. Cell Sci. 124, 2861–2871. [PubMed: 21807950]

Osterwalder T, Yoon KS, White BH, and Keshishian H (2001). A conditional tissue-specific transgene expression system using inducible GAL4. Proc. Natl. Acad. Sci. U S A 98, 12596–12601. [PubMed: 11675495]

Owusu-Ansah E, and Banerjee U (2009). Reactive oxygen species prime *Drosophila* haematopoietic progenitors for differentiation. Nature 461, 537–541. [PubMed: 19727075]

Peifer M (1995). Cell adhesion and signal transduction: the Armadillo connection. Trends Cell Biol. 5, 224–229. [PubMed: 14732126]

Phelps CB, and Brand AH (1998). Ectopic gene expression in *Drosophila* using GAL4 system. Methods 14, 367–379. [PubMed: 9608508]

Psathaki OE, Dehnen L, Hartley PS, and Paululat A (2018). *Drosophila* pericardial nephrocyte ultrastructure changes during ageing. Mech. Ageing Dev. 173, 9–20. [PubMed: 29702130]

Rotstein B, and Paululat A (2016). On the morphology of the *Drosophila* heart. J. Cardiovasc. Dev. Dis 3, E15. [PubMed: 29367564]

Rugendorff A, Younossi-Hartenstein A, and Hartenstein V (1994). Embryonic origin and differentiation of the *Drosophila* heart. Rouxs Arch. Dev. Biol 203, 266–280.

Shearin HK, Macdonald IS, Spector LP, and Stowers RS (2014). Hexameric GFP and mCherry Reporters for the *Drosophila* GAL4, Q, and LexA Transcription Systems. Genetics 196, 951–960. [PubMed: 24451596]

Shimokawa H (2013). Reactive oxygen species promote vascular smooth muscle cell proliferation. Circ. Res 113, 1040–1042. [PubMed: 24115068]

Skaer HL, and Maddrell SHP (1987). How are invertebrate epithelia made tight. J. Cell Sci. 88, 139–141.

Smith TK, and Bader DM (2007). Signals from both sides: control of cardiac development by the endocardium and epicardium. Semin. Cell Dev. Biol 18, 84–89. [PubMed: 17267246]

Struhl G, and Basler K (1993). Organizing activity of wingless protein in *Drosophila*. Cell 72, 527–540. [PubMed: 8440019]

Taverne YJHJ, Bogers AJJC, Duncker DJ, and Merkus D (2013). Reactive oxygen species and the cardiovascular system. Oxid. Med. Cell. Longev 2013, 862423. [PubMed: 23738043]

Tepass U, Tanentzapf G, Ward R, and Fehon R (2001). Epithelial cell polarity and cell junctions in *Drosophila*. Annu. Rev. Genet 35, 747–784. [PubMed: 11700298]

Tutor AS, Prieto-Sánchez S, and Ruiz-Gómez M (2014). Src64B phosphorylates Dumbfounded and regulates slit diaphragm dynamics: *Drosophila* as a model to study nephropathies. Development 141, 367–376. [PubMed: 24335255]

Vara D, and Pula G (2014). Reactive oxygen species: physiological roles in the regulation of vascular cells. Curr. Mol. Med 14, 1103–1125. [PubMed: 24894168]

Ward RE 4th, Lamb RS, and Fehon RG (1998). A conserved functional domain of *Drosophila* coracle is required for localization at the septate junction and has membrane-organizing activity. J. Cell Biol. 140, 1463–1473. [PubMed: 9508778]

Weavers H, Prieto-Sánchez S, Grawe F, Garcia-López A, Artero R, Wilsch-Braüninger M, Ruiz-Gómez M, Skaer H, and Denholm B (2009). The insect nephrocyte is a podocyte-like cell with a filtration slit diaphragm. Nature 457, 322–326. [PubMed: 18971929]

Wigglesworth VB (1970). The pericardial cells of insects: analogue of the reticuloendothelial system. J. Reticuloendothel. Soc 7, 208–216. [PubMed: 5436238]

Wilmes AC, Klinke N, Rotstein B, Meyer H, and Paululat A (2018). Biosynthesis and assembly of the Collagen IV-like protein Pericardin in *Drosophila melanogaster*. Biol. Open 7, 7.

Woods DF, Wu JW, and Bryant PJ (1997). Localization of proteins to the apico-lateral junctions of *Drosophila* epithelia. Dev. Genet 20, 111–118. [PubMed: 9144922]

Wu VM, Schulte J, Hirschi A, Tepass U, and Beitel GJ (2004). Sinuous is a *Drosophila* claudin required for septate junction organization and epithelial tube size control. J. Cell Biol. 164, 313–323. [PubMed: 14734539]

Xu C, Tang HW, Hung RJ, Hu Y, Ni X, Housden BE, and Perrimon N (2019). The septate junction protein Tsp2A restricts intestinal stem cell activity via endocytic regulation of aPKC and Hippo signaling. Cell Rep. 26, 670–688.e6. [PubMed: 30650359]

Yi P, Johnson AN, Han Z, Wu J, and Olson EN (2008). Heterotri-meric G proteins regulate a noncanonical function of septate junction proteins to maintain cardiac integrity in *Drosophila*. Dev. Cell 15, 704–713. [PubMed: 19000835]

Zecca M, and Struhl G (2007a). Control of *Drosophila* wing growth by the vestigial quadrant enhancer. Development 134, 3011–3020. [PubMed: 17634191]

Zecca M, and Struhl G (2007b). Recruitment of cells into the *Drosophila* wing primordium by a feed-forward circuit of vestigial autoregulation. Development 134, 3001–3010. [PubMed: 17634192]

Zhang F, Zhao Y, and Han Z (2013). An in vivo functional analysis system for renal gene discovery in *Drosophila* pericardial nephrocytes. J. Am. Soc. Nephrol 24, 191–197. [PubMed: 23291470]

Zhuang S, Shao H, Guo F, Trimble R, Pearce E, and Abmayr SM (2009). Sns and Kirre, the *Drosophila* orthologs of Nephrin and Neph1, direct adhesion, fusion and formation of a slit diaphragm-like structure in insect nephrocytes. Development 136, 2335–2344. [PubMed: 19515699]

Highlights

- Cora and Kune are septate junction proteins with a non-barrier role in *Drosophila*
- Cora and Kune levels are controlled by ROS-p38 signaling in pericardial cells (PCs)
- Cora and Kune mediate ROS-p38 signaling in PCs to maintain proper heart function
- Kune regulates its expression between adjacent cells in the heart but not in epithelia

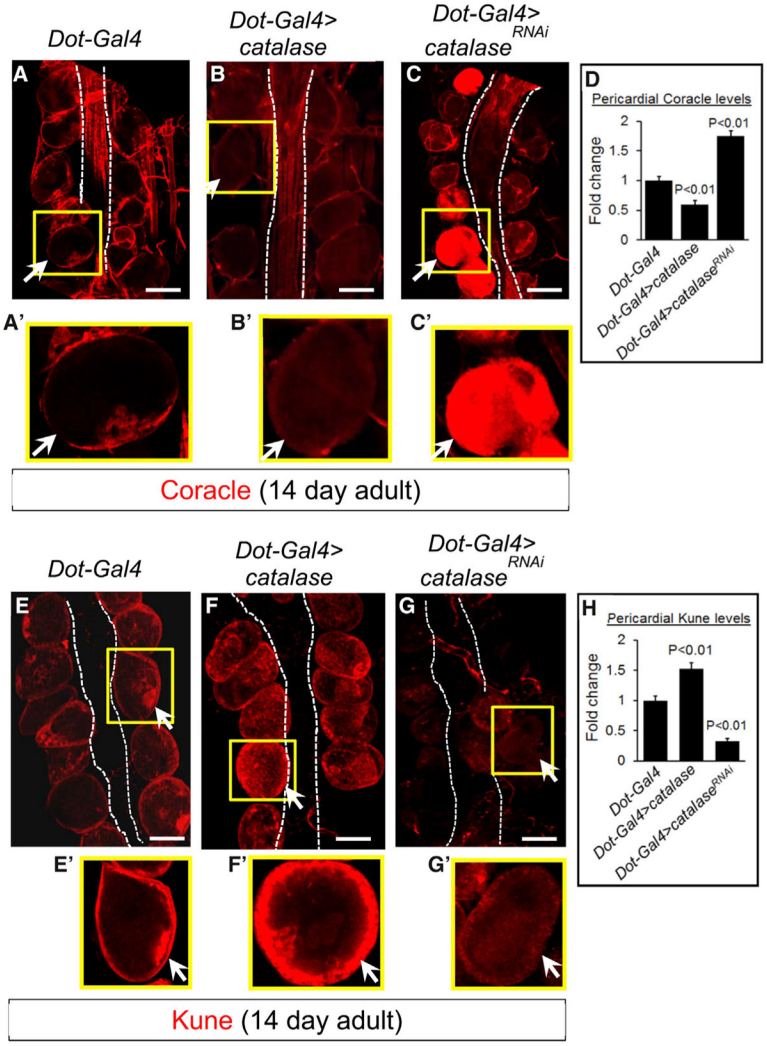

Figure 1. ROS Control Cora and Kune Levels in Pericardial Cells (PCs)

(A–C and E–G) Representative confocal images (20×) of Cora staining (red, A–C) and Kune staining (red, E–G) in fixed heart preparations from 14-day- old control flies (A and E), flies with PC-specific overexpression (B and F) or knockdown of *catalase* (C and G). For each heart, a representative PC (yellow box) is shown in a magnified (40×) blowout box in (A′)–(C′) and (E′)–(G′). Arrow denotes the same position of the PC in each yellow box and the corresponding blowout box. Dotted lines outline the myocardial tubes. Scale bar, 50 μm.

(D and H) Graphical quantification of pericardial Cora (D) and Kune (H) immunofluorescence with the mean intensity for each genotype normalized to that of control (*Dot-Gal4*; set at 1.0). For each genotype, approximately 10 PCs were analyzed from each of three adult flies.

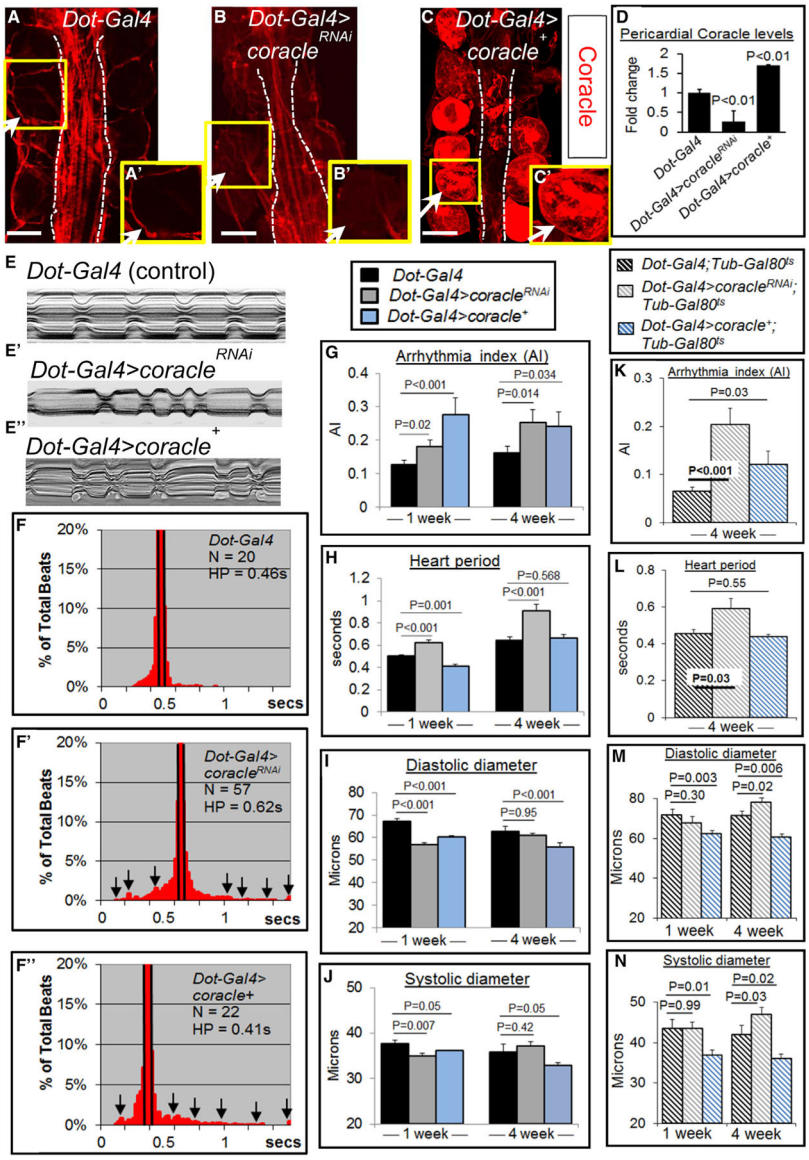

Figure 2. Loss- or Gain-of-Function of Cora in Pericardial Cells (PCs) Elicits Cardiac Dysfunction

(A–C) Representative confocal images (20×) of Cora staining (red) in fixed heart preparations from 1-week-old control flies (A), flies with PC-specific knockdown of *cora* (B), or overexpression of wild-type *cora* (C). For each heart, a representative PC (yellow box) is shown in a magnified (40×) blowout box in (A′), (B′), or (C′). Arrow denotes the same position of the PC in each yellow box and the corresponding blowout box. Dotted lines outline the myocardial tubes. Scale bar, 50 μm.

(D) Graphical quantification of Cora immunofluorescence in PCs with the mean intensity for each genotype normalized to that of the control (*Dot-Gal4*; set at 1.0). For each genotype, approximately 10 PCs were analyzed from each of three adult flies.

(E–F′) Representative 5 s M-mode traces (E–E′) and combined histograms showing the distribution of heart period (HP; F–F′) from 1-week-old flies of the indicated genotypes. Arrows indicate the broader distribution of HPs (F″ and F′) compared with control (F). N in

histograms indicates the number of flies analyzed. (G–J) AI (G), HP (H), and diastolic (I) and systolic (J) diameters in 1- and 4-week-old flies.
(K–N) AI (K), HP (L), and diastolic (M) and systolic (N) diameters in 1- and 4-week-old flies of the indicated genotypes. Results are mean ± SEM of 20–40 flies; p values are from Student's t test.

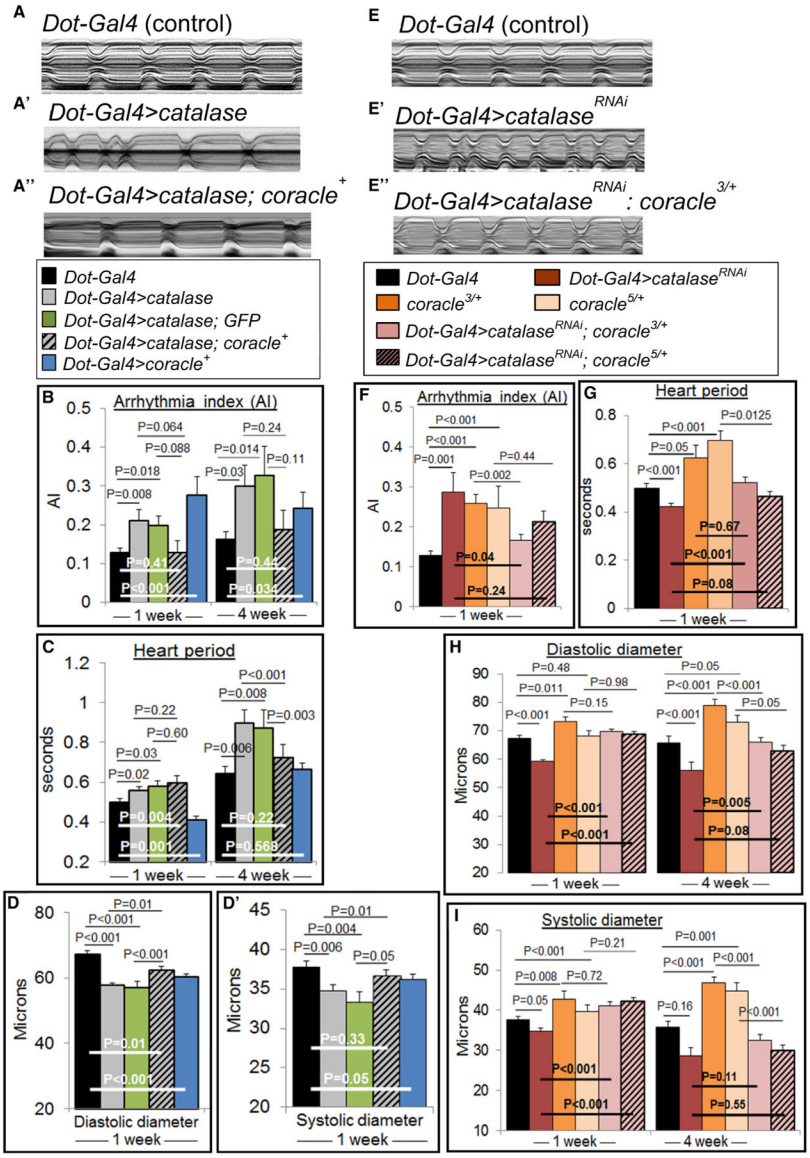

Figure 3. Cora Acts Downstream of ROS in Pericardial Cells (PCs) to Regulate Cardiac Function

(A–A″) Representative 5 s M-mode traces from 1-week old control flies (A), flies with PC-specific overexpression of catalase (A′), and flies with PC-specific co-overexpression of catalase and Cora (A″).

(B–D′) AI (B), HP (C), and diastolic (D) and systolic (D′) diameters in 1- and/or 4-week-old flies. Results are mean ± SEM of 30–40 flies; p values are from Student's t test.

(E–E″) Representative 5 s M-mode traces from 1-week-old control flies (E), flies with PC-specific knockdown of *catalase* (E′), or flies with PC-specific knockdown of *catalase* and are heterozygous for a *coracle* mutation (E″).

(F–I) AI (F), HP (G), and diastolic (H) and systolic (I) diameters in 1- and 4-week-old flies of the indicated genotypes. Results are mean ± SEM of 30–40 flies; p values are from Student's t test.

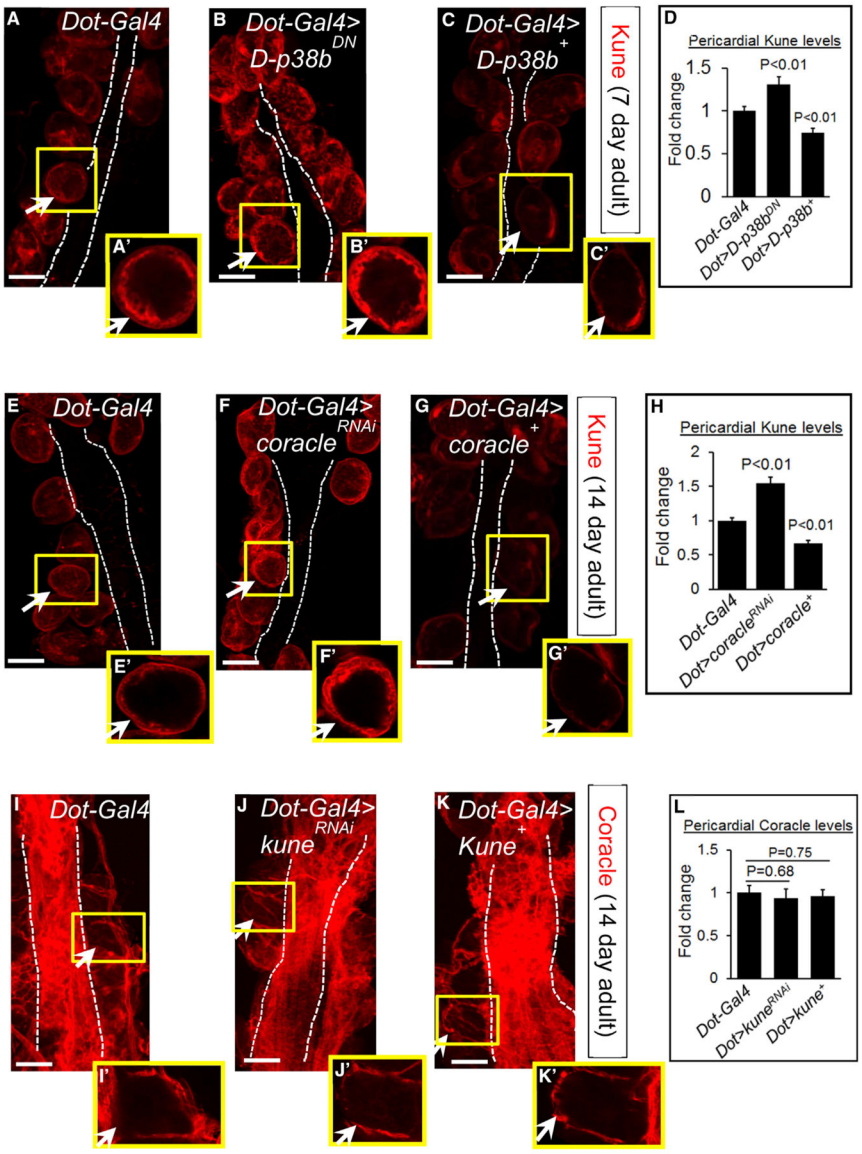

Figure 4. D-p38 and Cora Regulate Kune Content in Pericardial Cells (PCs)

(A–L) Representative confocal images (20×) of Kune and Cora staining (red) in fixed heart preparations from 7-day-old (A–D) or 14-day-old (E–L) flies of the indicated genotypes. In all cases, a representative PC within each heart tube (yellow box) is shown in a magnified (403) blowout box in (A′)–(C′), (E′)–(G′), and (I′)–(K′). Arrows denote the same position of the PC in each yellow box and the corresponding blowout box. Dotted lines indicate the boundary between PCs and the neighboring myocardial tubes. Scale bar, 50 μm.

Graphical quantification of pericardial Kune (D and H) or Cora (L) immunofluorescence in adult hearts with the mean intensity for each genotype normalized to that of the control (*Dot-Gal4*; set at 1.0). For each genotype, approximately 10 PCs were analyzed from each of three adult flies.

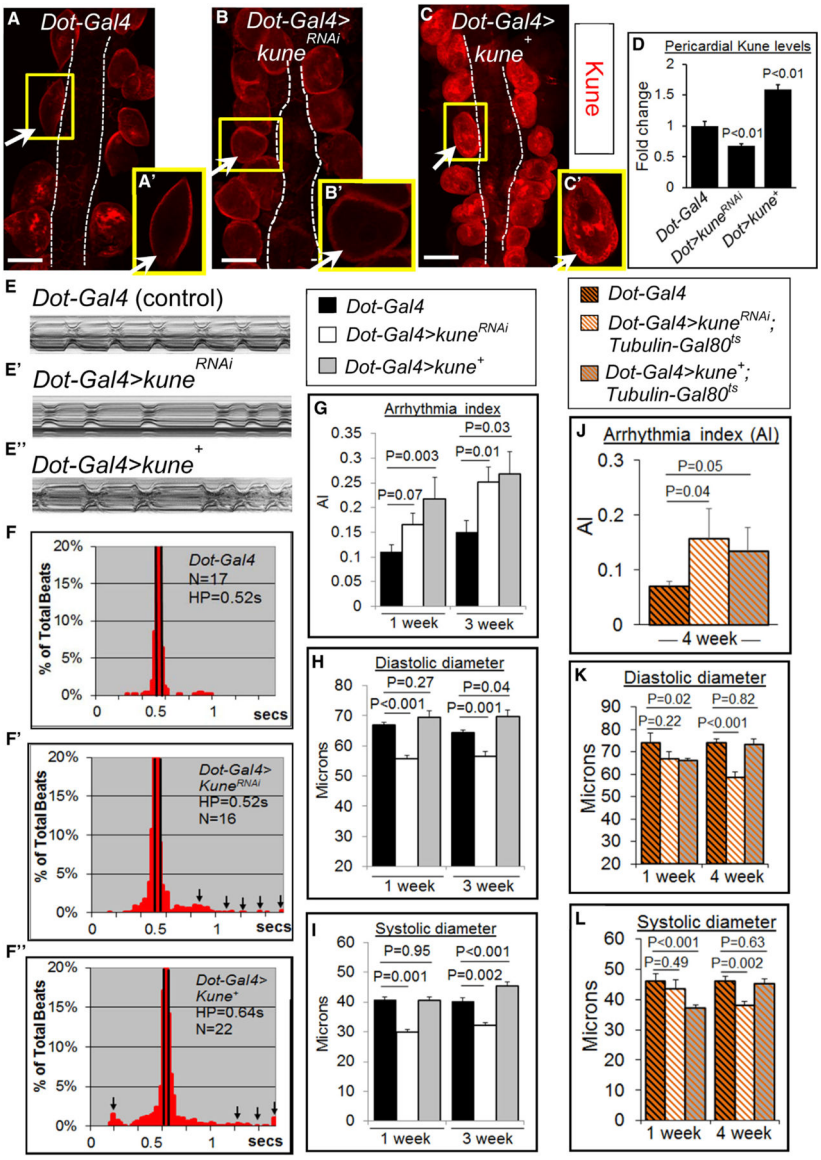

Figure 5. Loss- or Gain-of-Function of Kune in Pericardial Cells (PCs) Causes Cardiac Dysfunction

(A–C) Representative confocal images (20×) of Kune staining (red) in fixed heart preparations from 7-day-old control flies (A), flies with PC-specific knockdown of *kune* (B), and flies with PC-specific overexpression of wild-type Kune (C). In all cases, a representative PC within each heart tube (yellow box) is shown in a magnified (40×) blowout box in (A′), (B′), or (C′). Arrows denote the same position of the PC in each yellow box and the corresponding blowout box. Dotted lines indicate the boundary between PCs and the neighboring myocardial tubes. Scale bar, 50 μm.

(D) Graphical quantification of pericardial Kune immunofluorescence in adult hearts with the mean intensity for each genotype normalized to that of the control (*Dot-Gal4*; set at 1.0). For each genotype, approximately 10 PCs were analyzed from each of three adult flies.

(E–F″) Representative 5 s M-mode traces (E–E″) and combined histograms showing the distribution of HP (F–F″) from 1-week-old flies of the indicated genotypes. Arrows in

combined histograms (F′ and F″) indicate the broader distribution of HPs compared with control (F). N in histograms indicates the number of flies analyzed.

(G–I) AI (G) and diastolic (H) and systolic (I) diameters in 1- and 3-week-old flies of the indicated genotypes.

(J–L) AI (J) and diastolic (K) and systolic (L) diameters in 1- and 4-week-old flies of the indicated genotypes. Results are mean ± SEM of 20–40 flies; p values are from Student's t test.

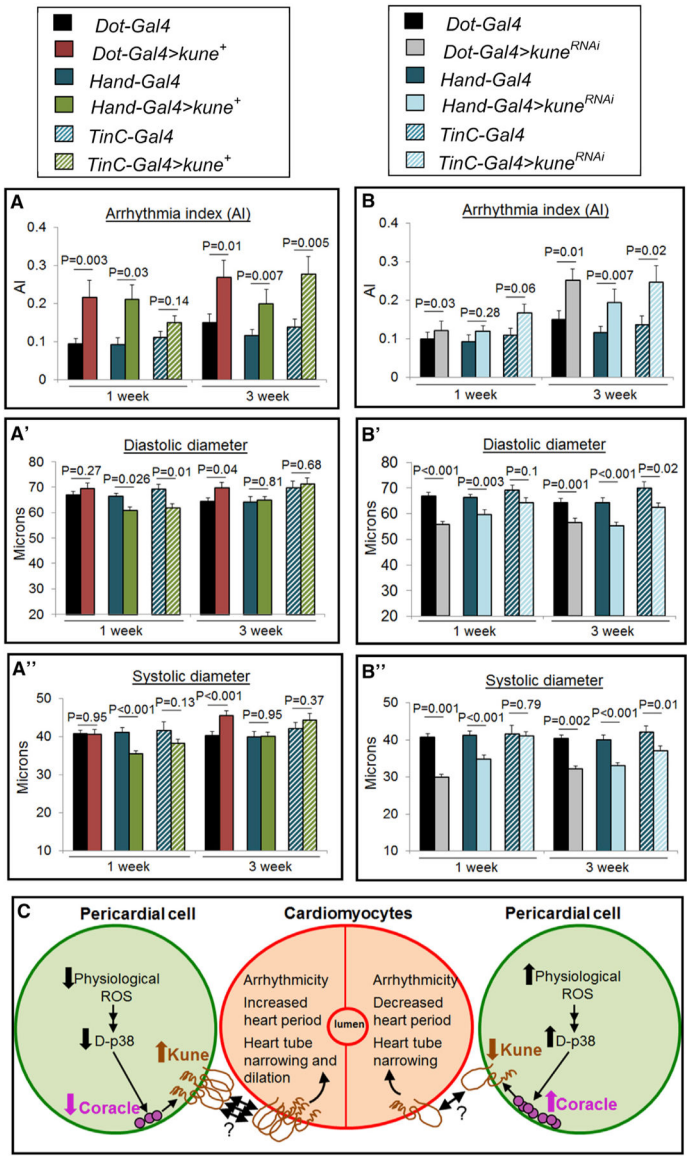

Figure 6. Pericardial and Myocardial Kune Regulate Cardiac Function in a Similar Manner

(A–A″) AI (A), diastolic diameter (A′), and systolic diameter (A″) in 1- and 3-week-old control flies and flies with PC- or CM-specific overexpression of wild-type Kune. (B–B″) AI (B), diastolic diameter (B′), and systolic diameter (B″) in 1- and 3-week-old control flies and flies with PC- or CM-specific knockdown of *kune*. (C) A model of how alterations in ROS-mediated signaling in PCs affect neighboring CM function and morphology (see Discussion).

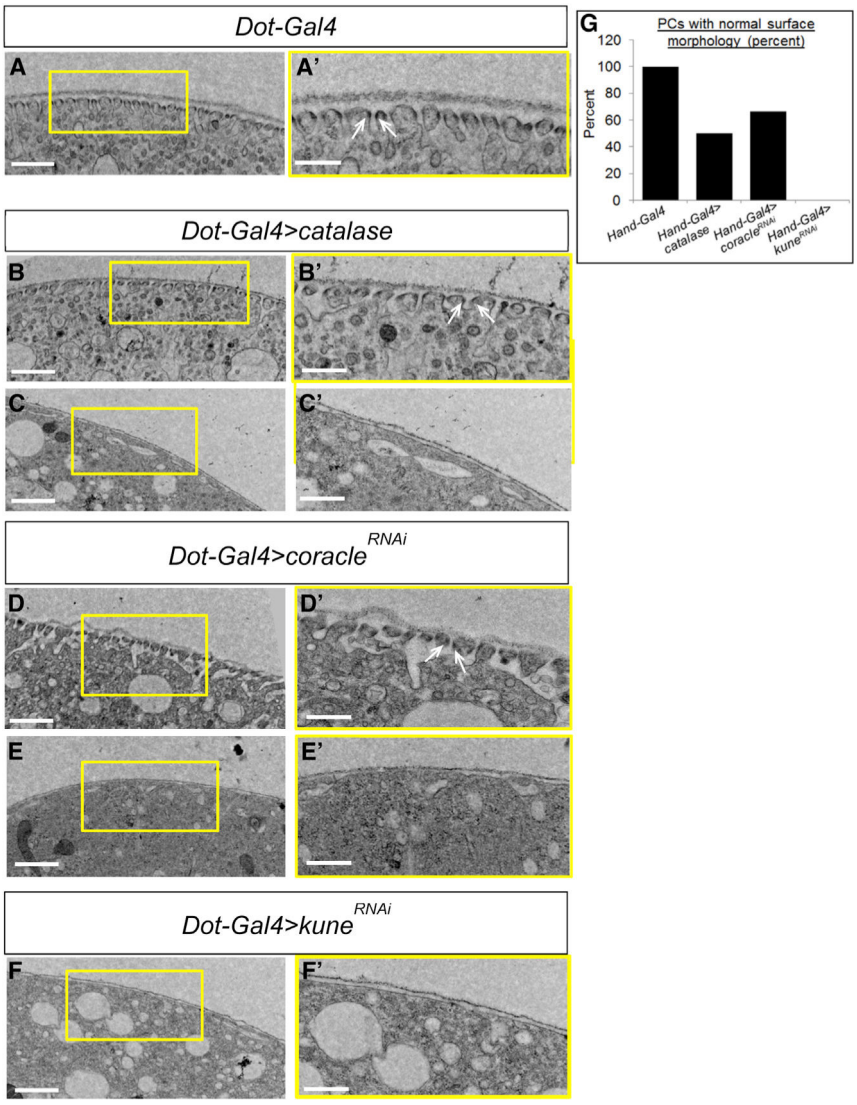

Figure 7. Surface Morphology of Pericardial Cells (PCs) is Disrupted by Alterations in ROS, Coracle, or Kune Level

(A–F) Ultrastructural morphology of PCs (2,500× magnification) in 1-week-old flies old control flies (A), flies with PC-specific overexpression of *catalase* (B and C), flies with PC-specific knockdown of *coracle* (D and E), or flies with PC-specific knockdown of *kune* (F). In all cases, a part of the PC (yellow box) is shown in a magnified (5,000×) blowout box in (A′)–(F′). White arrows denote the electron-dense slit diaphragm in the labyrinthine channel opening. Scale bars, 1 μm (A–F) and 500 nm (A′–F′).

(G) Percentage of PCs exhibiting intact labyrinthine channels and slit diaphragm uniformly throughout their surfaces. For each genotype, five to six PCs from two flies were analyzed.

KEY RESOURCES TABLE

REAGENT or RESOURCE	SOURCE	IDENTIFIER
Antibodies		
mouse anti-Cora	Developmental Studies Hybridoma Bank	C566.9; RRID:AB_1161642 and c615.16;RRID:AB_1161644
mouse anti-Nervana	Developmental Studies Hybridoma Bank	Nrv5F7; RRID:AB_528395
mouse anti-Disc large	Developmental Studies Hybridoma Bank	4F3; RRID:AB_528203
mouse anti-Armadillo	Developmental Studies Hybridoma Bank	N2 7A1; RRID:AB_528089
mouse anti-ERM-1	Developmental Studies Hybridoma Bank	ERM-1; RRID:AB_10584795
mouse anti-Talin	Developmental Studies Hybridoma Bank	E16B; RRID:AB_10683995
mouse anti-Contactin	Developmental Studies Hybridoma Bank	3.1C12; RRID:AB_2229763
mouse Anti-GFP	Abcam	Cat# ab13970; RRID:AB_300798
Rabbit anti-Kune	Greg Beitel and Mikio Furuse	Nelson et al., 2010
Rabbit anti-Sinuous	Greg Beitel	Wu et al., 2004
Rabbit anti-Neurexin-IV	Manzoor Bhat	Li et al., 2007
Rabbit anti-Megatrachea	Reinhard Schuh	Behr et al., 2003
Cy3-conjugated AffiniPure Donkey Anti-Mouse IgG (H+L)	Jackson ImmunoResearch Labs	Cat# 715-165-151; RRID:AB_2315777
Cy3-conjugated AffiniPure Donkey Anti-Rabbit IgG (H+L)	Jackson ImmunoResearch Labs	Code# 715-165-152; RRID:AB_2307443
Normal Donkey Serum	Jackson ImmunoResearch Labs	Code# 017-000-001; RRID:AB_2337254
Anti-Mouse, IgG (Goat), HRP-labeled	Perkin Elmer	NEF 822001 EA; RRID:AB_2650498
Anti-Rabbit, IgG (Goat), HRP-labeled	Perkin Elmer	NEF 812001 EA; RRID:AB_2571640
Chemicals, Peptides, and Recombinant Proteins		
Dihydroethidium	Molecular Probes, Invitrogen	Cat# D11347
DMSO	Sigma	Cat# 276855
L-glucose	Sigma	Cat# G5500
Sucrose	Sigma	Cat# S0389
Formaldehyde	Fisher Scientific	Cat# F79-500
Glacial acetic acid	Sigma	Cat# 1005706
Picric acid	Sigma	Cat# 197378
Paraformaldehyde (EM grade)	Electron Microscopy Sciences	Cat# 157-4-100
Glutaraldehyde (EM Grade)	Electron Microscopy Sciences	Cat# 111 −30-8
EMS resin	Electron Microscopy Sciences	Cat# 13940
N-Benzyldimethylamine (BDMA)	Electron Microscopy Sciences	Cat# 103-83-3
Uranyl Acetate	Electron Microscopy Sciences	Cat# 22400
Lead Citrate	Electron Microscopy Sciences	Cat# 17800
Osmium tetroxide	Sigma	Cat# O5500
Acetone (EM Grade)	Polysciences Inc.	Cat# 01921
Propylene Oxide (EM Grade)	Polysciences Inc.	Cat# 00236-1

REAGENT or RESOURCE	SOURCE	IDENTIFIER
Methanol (EM Grade)	Polysciences Inc.	Cat# 08032-6
Vectashield mounting medium	Vector laboratories	Cat# H-1000
Experimental Models: Organisms/Strains		
w^{1118}	Bloomington	BDSC # 6326
UAS-catalase	Bloomington	BDSC # 24621
UAS-sod1	Bloomington	BDSC # 24750
UAS-sod2	Bloomington	BDSC # 24494
UAS-D-p38bDN	Bloomington	BDSC # 59005
UAS-coracle^{+}	Bloomington	BDSC # 16848
UAS-Nrx-IV^{RNAi}	Bloomington	BDSC # 28715
UAS-Nrv2^{RNAi}	Bloomington	BDSC # 37495
UAS-catalase^{RNAi}	VDRC	v103581
UAS-sod1^{RNAi}	VDRC	v31551
UAS-sod2^{RNAi}	VDRC	v42162
UAS-kune^{+}	Greg Beitel	Nelson et al., 2010
UAS-p38b^{+}	Jianming Chen	Chen et al., 2010
D-p38a^{13}	Jianming Chen	Chen et al., 2010
D-p38b^{156A}	Jianming Chen	Chen et al., 2010
Dot-Gal4	N/A	Kimbrell et al., 2002
Sns-Gal4	Susan Abmayr	Zhuang et al., 2009
Hand-Gal4	Lauren Perrin	Lee et al., 2017
TinCΔ4-Gal4	Rolf Bodmer	Lo and Frasch., 2001
yw flip; Tubulin > GFPy^{+} > Gal4, 20XUAS. 6XGFP	Gary Struhl	Shearin et al., 2014
Software and Algorithms		
Simple PCI	Compix	N/A
MATLAB-based image analysis	Karen Ocorr	Fink et al., 2009